RSC Advances

PAPER

View Article Online
View Journal | View Issue

CrossMark click for updates

Cite this: *RSC Adv.*, 2015, **5**, 4681

Synthesis, crystal structures, and spectral properties of double *N*-alkylated dimethine cyanine dyes and their interactions with biomolecules and living cells†

Hongliang Jia,[a] Ying Lv,[a] Shu Wang,[a] Dan Sun[b] and Lanying Wang*[a]

Received 19th September 2014
Accepted 27th November 2014

DOI: 10.1039/c4ra10741a

www.rsc.org/advances

Six new double *N*-alkylated dimethine cyanine dyes were synthesized and the crystal structures of two of the dyes were analyzed by X-ray diffraction. The investigation of the spectral properties of the dyes in different solvents indicated that the absorption maxima of the dyes decreased with the increase of the basicity of the heterocyclic nucleus, and the increase of the solvent dielectric constants of the protonic solvents and non-protonic solvents. The six dyes all emitted fluorescence, and had a larger Stokes shift in water. The interaction between the dye molecules and the six biological molecules showed that one dye exhibited a larger enhancement of fluorescent quantum yield in the presence of DNA. Investigation of the cytotoxicity and cell staining of the selected dye showed that the dye had virtually no toxicity at the application dose and duration used and that it could stain cytoplasm, suggesting its potential application as a fluorescent reagent with which to observe and analyze the characteristics of living cells.

1. Introduction

Cyanine dyes, a class of synthetic functional dyes with two heteroaromatic rings joined by a methine chain, are widely used in materials,[1–4] biomedicine[5–8] and other fields[9] because of their high extinction coefficients, tunable absorption/emission spectra, and a moderate-to-high fluorescence quantum yield. Monomethine cyanine dyes are important in the family of cyanine dyes, and have also been used in the biomedical field because of their high affinity towards certain biological molecules,[10] such as in nucleic acid detection,[11–13] as a protein-based fluoromodule,[14] for DNA sequencing[15–17] and cell imaging[18,19] and so on. Monomethine cyanine dyes are usually prepared by the condensation reaction of a heterocyclic quaternary salt bearing an active methyl group, with another quaternary salt of 2- or 4-alkylthio heterocyclic compounds,[20] and the reaction is accompanied by the formation of a thiol molecule. This will pollute the environment and does not comply with the concept of green chemistry. In addition, the processes of separation and purification of the products are relatively complex and cumbersome, and the yields are usually low.[21] Compared with monomethine cyanine dyes, dimethine cyanine dyes, which are prepared from a heterocyclic quaternary salt having an active methyl group *via* a condensation reaction with an aromatic heterocyclic aldehyde, are easily synthesized and purified with high yields and are produced by an environmentally friendly pathway. More importantly, the dimethine cyanine dyes have similar properties to monomethine cyanine dyes, such as good spectral properties and affinity for biological molecules.[11,22,23] Therefore, research on the synthesis and application of dimethine cyanine dyes is of great interest and importance. Wang and Chang[24] reported on the combinatorial synthesis of benzimidazolium dyes, studied their interaction with nucleotides, and discovered the first turn-on fluorescent guanosine triphosphate sensor. In addition, the research team synthesized a type of dimethine cyanine dye,[25] which had low cell cytotoxicity, low phototoxicity, high photostability, and found that it was suitable for detecting an *in vitro* RNA response and for live cell nuclear imaging. Abd El-Aal *et al.*[26] synthesized β-substituted dimethine cyanine dyes, and discussed the relationship between the properties and structures of the dyes. Deligeorgiev *et al.*[27] described three new general procedures for the synthesis of dimethine cyanine dyes using uncatalysed Knoevenagel condensation, which had several virtues, such as high yields, highly pure final dyes, short reaction time and an environmentally friendly method, and investigated the spectral properties of the novel dyes. In previous work,[23,28] we synthesized a series of dimethine cyanine dyes and investigated, both experimentally and theoretically, the absorption and

[a]*Key Laboratory of Synthetic and Natural Functional Molecule Chemistry, Ministry of Education, College of Chemistry and Materials Science, Northwest University, Xi'an 710069, P. R. China. E-mail: wanglany@nwu.edu.cn; Fax: +86 29 81535026; Tel: +86 29 81535026*

[b]*Institute of Photonics & Photon-Technology, Northwest University, Xi'an 710069, P. R. China*

† Electronic supplementary information (ESI) available. CCDC 851574 and 822789. For ESI and crystallographic data in CIF or other electronic format see DOI: 10.1039/c4ra10741a

fluorescence properties of these dyes. They were also studied as fluorescent dyes for DNA or bovine serum albumin (BSA) detection, and it was found that fluorescent intensity was increased when the dyes were bound to DNA. Recently, the synthesis of a series of dimethine cyanine dyes was reported and their properties as fluorescent probes for living cell imaging and flow cytometry were investigated. The results showed that some dyes could penetrate an intact cell membrane and stain the cell nucleus, and they could also be applied in flow cytometry.[29] However, from the research mentioned previously it was found that the reported dimethine cyanine dyes, with heterocyclic nitrogen links with hydrogen, are susceptible to the external environment[30] and have a small Stokes shift.

In this paper, the synthesis of a series of new double *N*-alkylated dimethine cyanine dyes including *N*-methylation and *N*-benzylation (Scheme 1), which would have a large Stokes shift and resistance to environmental interference as well as good stability, was described. Their structures were identified using ultraviolet-visible (UV-vis) spectroscopy, proton nuclear magnetic resonance (^{1}H-NMR) spectroscopy, infrared spectroscopy (IR) and high-resolution mass spectroscopy (HRMS) and the structures of dyes **C2** and **C6** were characterized and analyzed by X-ray diffraction (XRD). The absorption and fluorescent spectra of these dyes in different solvents and their interaction with six biological molecules was investigated, as well as their cytotoxicity and cell staining of the selected dye **C3** for their prospective uses as fluorescent reagents in the biomedical field.

2. Experimental

2.1 General

Commercially available reagents were used without additional purification. All solvents were of analytical grade. Melting points were measured using a XT-4 micromelting apparatus and were used uncorrected. IR spectra (cm^{-1}) were recorded on a Bruker Equinox 55 spectrometer. The absorption spectra were recorded on a Purkinje General TU-1900 UV-vis spectrometer. ^{1}H-NMR spectra were recorded at 400 MHz on a Varian Inova 400 spectrometer and chemical shifts were reported relative to the internal standard, tetramethylsilane. HRMS was recorded on a Bruker micrOTOF-Q II electrospray ionisation – quadrupole time-of-flight (ESI-QTOF) liquid chromatography-mass spectroscopy (LC-MS) spectrometer. High performance liquid chromatography (HPLC) was performed using a Shimadzu LC-20AD. Single crystal XRD data were collected using a Bruker SMART APEX II charge coupled device (CCD) detector for X-ray crystallography. Fluorescence imaging was carried out on a Nikon A1 laser scanning confocal microscope. The water soluble tetrazolium (WST) assay was conducted using a BioTek ELx 800 microplate reader. Cell lines were cultured in a Thermo Scientific Forma 3111 water-jacketed carbon dioxide incubator.

2.2 Preparation of the intermediates A1–A6 and B1

2.2.1 Preparation of the intermediates A1–A6. 2,3-Dimethyl benzothiazolium iodide salt (**A1**), 1,2,3-trimethyl benzimidazolium iodide salt (**A2**), 7-chloro-1,2-dimethyl quinolinium iodide

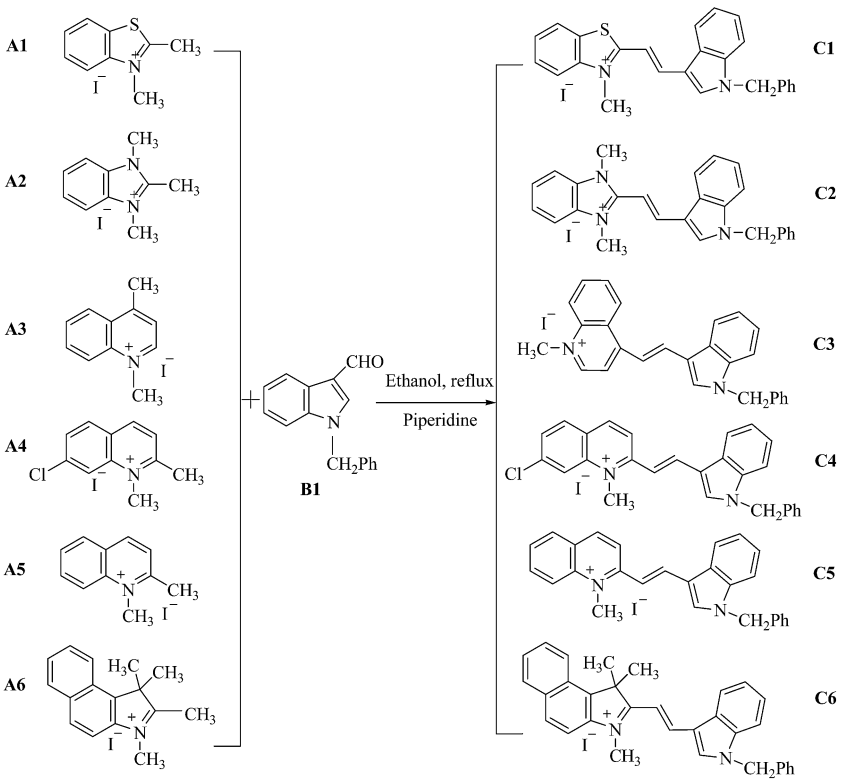

Scheme 1 Synthesis of dyes **C1–C6**.

salt (**A4**), and 1,2-dimethyl quinolinium iodide salt (**A5**) were synthesized according to methods in the literature.[29] 1,4-Dimethyl quinolinium iodide salt (**A3**),[31] and 1,2,3,3-tetramethyl-4,5-benzindolium iodide salt (**A6**)[32] were also prepared according to methods in the literature.

2.2.2 Preparation of the intermediate B1. *N*-Benzyl-3-indole formaldehyde (**B1**) was prepared according to a modified procedure from the literature.[33] Indole-3-carboxaldehyde (0.14 g, 1.0 mmol) was dissolved in 10.0 mL of *N*,*N*-dimethylformamide (DMF) at room temperature, and 40% of sodium hydride (0.06 g, 1.0 mmol) was added with stirring at 0–5 °C for 0.5–1 h, then the benzyl chloride (0.25 g, 2.0 mmol) was added. The resulting mixture was stirred at room temperature for 24 h, then filtered and the DMF was evaporated off. The product was recrystallized from ethanol (EtOH) to give **B1** (0.21 g, 87.5%) as faint yellow crystals, melting point (mp) 106–107 °C (literature mp 107 °C).

2.3 Synthesis of double *N*-alkylated dimethine cyanine dyes (C1–C6)

2.3.1 Preparation of dyes C1–C6. Dimethine cyanine dyes (**C1–C6**) were prepared as shown in Scheme 1. Equimolar amounts of heterocycle intermediates **A1–A6** (1.0 mmol) and **B1** (1.0 mmol) were dissolved in anhydrous EtOH. A few drops of piperidine were added and the reaction mixture was stirred under reflux for 3–6 h. The progress of the reaction was monitored using UV-vis spectroscopy. After cooling, the resulting precipitate was filtered off and recrystallized from methanol (MeOH) (**C2**) or EtOH (**C1**, **C3–C6**). The reaction details and yields of dyes **C1–C6** are listed in Table 1.

2.3.2 Structural confirmation

*1-Methyl-2-[1-benzyl-3-indole-(E)-ethenyl]benzothiazolium iodide salt (**C1**).* UV-vis (MeOH) λ_{max}: 471.0 nm. ^{1}H-NMR (400 MHz, deuterated dimethyl sulfoxide (DMSO-d_6)) δ (ppm): 4.28 (s, 3H, N^+CH_3), 5.60 (s, 2H, NCH_2Ph), 7.33–7.38 (m, 7H, ArH), 7.52 (d, 1H, J = 15.6 Hz, CH=CH), 7.68–7.72 (m, 2H, ArH), 7.79–7.82 (m, 1H, ArH), 8.14 (d, 1H, J = 8.0 Hz, ArH), 8.29–8.34 (m, 2H, ArH), 8.42 (d, 1H, J = 15.6 Hz, CH=CH), 8.58 (s, 1H, pyrrole-H). IR (KBr) ν: 3045, 3009 (m, $\nu_{=C-H}$), 2927 (m, ν_{C-H}), 1536, 1448 (s, $\nu_{C=C}$, $\nu_{C=N}$), 1399, 1366, 1343, 1220, 1107 (m, δ_{C-H}), 944, 837, 747, 719 (m, $\delta_{=C-H}$) cm^{-1}. HRMS (TOF-MS ESI) calculated for $C_{25}H_{21}N_2S^+$: 381.1420; found: 381.1397.

*1,3-Dimethyl-2-[1-benzyl-3-indole-(E)-ethenyl]benzimidazolium iodide salt (**C2**).* UV-vis (MeOH) λ_{max}: 376.0 nm. ^{1}H-NMR (400 MHz, DMSO-d_6) δ (ppm): 4.15 (s, 6H, NCH_3, N^+CH_3), 5.57 (s, 2H, NCH_2Ph), 7.18 (d, 1H, J = 16.0 Hz, CH=CH), 7.30–7.37 (m, 7H, ArH), 7.64–7.68 (m, 3H, ArH), 8.04 (d, 1H, J = 16.0 Hz, CH=CH), 8.00–8.06 (m, 2H, ArH), 8.21–8.23 (m, 1H, ArH), 8.33 (s, 1H, pyrrole-H). IR (KBr) ν: 3016 (m, $\nu_{=C-H}$), 2931 (m, ν_{C-H}), 1598, 1502, 1457 (s, $\nu_{C=C}$, $\nu_{C=N}$), 1349, 1186 (m, δ_{C-H}) 964, 738 (m, $\delta_{=C-H}$) cm^{-1}. HRMS (TOF-MS ESI) calculated for $C_{26}H_{24}N_3^+$: 378.1965; found: 378.1941.

*1-Methyl-4-[1-benzyl-3-indole-(E)-ethenyl]quinolinium iodide salt (**C3**).* UV-vis (MeOH) λ_{max}: 503.0 nm. ^{1}H-NMR (400 MHz, DMSO-d_6) δ (ppm): 4.46 (s, 3H, N^+CH_3), 5.59 (s, 2H, NCH_2Ph), 7.31–7.37 (m, 7H, ArH), 7.65–7.67 (m, 1H, ArH), 8.01 (d, 1H, J = 8.0 Hz, ArH), 8.04 (d, 1H, J = 16.0 Hz, CH=CH), 8.21–8.24 (m, 1H, ArH), 8.28–8.30 (m, 1H, ArH), 8.35 (d, 1H, J = 8.0 Hz, ArH), 8.46 (d, 1H, J = 8.0 Hz, ArH), 8.51 (s, 1H, pyrrole-H), 8.55 (d, 1H, J = 16.0 Hz, CH=CH), 8.96 (d, 1H, J = 8.0 Hz, ArH), 9.15 (d, 1H, J = 8.0 Hz, ArH). IR (KBr) ν: 3058 (m, $\nu_{=C-H}$), 2921 (w, ν_{C-H}), 1556, 1515, 1482 (m, $\nu_{C=C}$, $\nu_{C=N}$), 1394, 1295, 1157 (m, δ_{C-H}), 964, 738 (m, $\delta_{=C-H}$) cm^{-1}. HRMS (TOF-MS ESI) calculated for $C_{27}H_{23}N_2^+$: 375.1856; found: 375.1840.

*7-Chloro-1-methyl-2-[1-benzyl-3-indole-(E)-ethenyl]quinolinium iodide salt (**C4**).* UV-vis (MeOH) λ_{max}: 491.0 nm. ^{1}H-NMR (400 MHz, DMSO-d_6) δ (ppm): 4.44 (s, 3H, N^+CH_3), 5.61 (s, 2H, NCH_2Ph), 7.33–7.40 (m, 7H, ArH), 7.56 (d, 1H, J = 16.0 Hz, CH=CH), 7.68–7.69 (m, 1H, ArH), 7.90 (d, 1H, J = 8.0 Hz, ArH), 8.26 (d, 2H, J = 8.0 Hz, ArH), 8.60–8.64 (m, 3H, ArH, pyrrole-H), 8.66 (d, 1H, J = 16.0 Hz, CH=CH), 8.81 (d, 1H, J = 8.0 Hz, ArH). IR (KBr) ν: 3002 (w, $\nu_{=C-H}$), 2921 (w, ν_{C-H}), 1581, 1506, 1457 (s, $\nu_{C=C}$, $\nu_{C=N}$), 1398, 1346, 1299, 1164 (m, δ_{C-H}), 956, 844, 740 (m, $\delta_{=C-H}$) cm^{-1}. HRMS (TOF-MS ESI) calculated for $C_{27}H_{22}N_2Cl^+$: 409.1466; found: 409.1448.

*1-Methyl-2-[1-benzyl-3-indole-(E)-ethenyl]quinolinium iodide salt (**C5**).* UV-vis (MeOH) λ_{max}: 479.0 nm. ^{1}H-NMR (400 MHz, DMSO-d_6) δ (ppm): 4.49 (s, 3H, N^+CH_3), 5.61 (s, 2H, NCH_2Ph), 7.33–7.38 (m, 7H, ArH), 7.59 (d, 1H, J = 16.0 Hz, CH=CH), 7.67–7.69 (m, 1H, ArH), 7.84–7.88 (m, 1H, ArH), 8.08–8.12 (m, 1H, ArH), 8.25–8.27 (m, 2H, ArH), 8.46 (d, 1H, J = 8.0 Hz, ArH), 8.56 (s, 1H, pyrrole-H), 8.62–8.66 (m, 2H, ArH, CH=CH), 8.84 (d, 1H, J = 8.0 Hz, ArH). IR (KBr) ν: 3064, 3019 (m, $\nu_{=C-H}$), 2925 (m, ν_{C-H}), 1585, 1511, 1455 (s, $\nu_{C=C}$, $\nu_{C=N}$), 1347, 1299, 1157, 1106 (m, δ_{C-H}), 958, 838, 750 (m, $\delta_{=C-H}$) cm^{-1}. HRMS (TOF-MS ESI) calculated for $C_{27}H_{23}N_2^+$: 375.1856; found: 375.1846.

*1,3,3-Trimethyl-2-[1-benzyl-3-indole-(E)-ethenyl]-4,5-benzindolium iodide salt (**C6**).* UV-vis (MeOH) λ_{max}: 489.0 nm. ^{1}H-NMR (400 MHz, DMSO-d_6) δ (ppm): 2.05 (s, 6H, $C(CH_3)_2$), 4.16 (s, 3H,

Table 1 The molecular formulas, reaction times, melting points, yields and appearance of C1–C6

Dye	Formula	Reaction time (h)	mp (°C)	Yield (%)	Appearance
C1	$C_{25}H_{21}N_2SI$	4.0	261–262	59	Orange solid
C2	$C_{26}H_{24}N_3I$	6.0	>300	77	Yellow acicular crystals
C3	$C_{27}H_{23}N_2I$	3.5	245–246	80	Red solid
C4	$C_{27}H_{22}N_2ICl$	4.0	236–237	50	Dark red power
C5	$C_{27}H_{23}N_2I$	3.5	269–270	84	Red solid
C6	$C_{32}H_{29}N_2I$	5.0	207–208	83	Red acicular crystals

N^+CH_3), 5.66 (s, 2H, NCH_2Ph), 7.26 (d, 1H, J = 16.0 Hz, CH=CH), 7.35–7.44 (m, 7H, ArH), 7.65 (d, 1H, J = 8.0 Hz, ArH), 7.77 (d, 2H, J = 8.0 Hz, ArH), 8.05 (d, 1H, J = 8.8 Hz, ArH), 8.18 (d, 1H, J = 8.0 Hz, ArH), 8.24 (d, 1H, J = 8.8 Hz, ArH), 8.33 (d, 1H, J = 8.0 Hz, ArH), 8.40 (d, 1H, J = 8.0 Hz, ArH), 8.76 (d, 1H, J = 16.0 Hz, CH=CH), 8.84 (s, 1H, pyrrole-H). IR (KBr) ν: 3091, 3033 (m, $\nu_{=C-H}$), 2995 (m, ν_{C-H}), 1563, 1498, 1457 (m, $\nu_{C=C}$, $\nu_{C=N}$), 1394, 1347, 1249, 1205, 1160, 1118 (m, δ_{C-H}), 939, 792, 744 (m, $\delta_{=C-H}$) cm^{-1}. HRMS (TOF-MS ESI) calculated for $C_{32}H_{29}N_2^+$: 441.2325; found: 441.2307.

2.4 Crystal data

Crystals suitable for X-ray analysis were obtained by the slow evaporation of a solution of the dyes in MeOH (**C2**) or EtOH (**C6**). All the measurements of the crystals were carried out on a Bruker SMART APEX II (CCD) detector for crystallography, equipped with graphite monochromated Mo Kα radiation (λ = 0.71073 nm), by using the ω scan technique at room temperature. The structures were solved by direct methods using SHELXS-97 software,[34] and refined using the full-matrix least-squares method on F^2 with anisotropic thermal parameters for all non-hydrogen atoms using SHELXL-97.[35] Hydrogen atoms were generated geometrically. Fig. 1 and 2 show the molecular structures with numbering systems of dyes **C2** and **C6**, respectively. The crystal data, details concerning data collection and structure refinement for dyes **C2** and **C6** are summarized in Table 2. The bond lengths, bond angles and torsion angles for dyes **C2** and **C6** are listed in Tables 3 and 4, respectively. The geometry of D–H···A hydrogen bonds for dyes **C2** are listed in Table 5. Parameters in crystallographic information framework (CIF) format are available as ESI.†

2.5 Measurements of the spectral properties of dyes

2.5.1 Measurements of the spectral properties of dyes in different solvents. The dye stock solutions (1×10^{-2} mol L^{-1} in dimethyl sulfoxide (DMSO)) were diluted with different solvents and resulted in working solutions of dyes (1×10^{-5} mol L^{-1}). The absorption and fluorescence emission spectra of these solutions were scanned at room temperature. The size of quartz cell and the slit width of excitation and emission spectra were 1 cm × 1 cm × 4 cm and 5.0 nm, respectively. The absorption and fluorescence spectral data are listed in Table 6.

2.5.2 Measurements of the spectral properties of dyes in the presence of biomolecules. The dye stock solutions with a concentration of 5×10^{-3} mol L^{-1} were prepared by dissolving the dyes in DMSO and were then further diluted with TE buffer consisting of 10 mmol L^{-1} Tris–HCl, 1 mmol L^{-1} EDTA at pH 7.5. The biomolecule stock solutions (200 μg mL^{-1}) were prepared by dissolving biomolecules (DNA, BSA, muramidase, amylase, bovine hemoglobin or chymotrypsin) in TE buffer. Working solutions of complexed biomolecule–dye were prepared by mixing dye stock solutions and biomolecule stock solutions, and further diluting them with TE buffer. The working concentrations of the dye solutions were 1×10^{-5} mol L^{-1} and 5×10^{-5} mol L^{-1} for dyes **C1** and **C2**, and 1×10^{-5} mol L^{-1} and 3×10^{-5} mol L^{-1} for dyes **C3**, **C4** and **C5**, and 1×10^{-5} mol L^{-1} and 5×10^{-6} mol L^{-1} for dye **C6**. The biomolecule concentrations in working solutions were 0, 4 and 10 μg mL^{-1}. All working solutions were prepared immediately before use. The measurement method was the same as that described previously. The results are shown in Table 7.

2.5.3 Preparation of dye–DNA solutions. The dye stock solution (1×10^{-4} mol L^{-1}) was prepared by dissolving dye **C1** in DMSO and diluting it further with TE buffer. The stock solution of DNA with a concentration of 200 μg mL^{-1} was prepared by dissolving DNA in TE buffer. Working solutions of complexed DNA–dye were prepared by mixing an aliquot of the dye stock solution with an aliquot of the DNA stock solutions, and diluting it further with TE buffer to obtain the required concentrations (DNA: 0, 2, 4, 6, 8, 10 and 12 μg mL^{-1}, dye **C1**: 1×10^{-5} mol L^{-1}).

2.6 Determination of cytotoxicity and cell staining

2.6.1 Cytotoxicity of dye C3. The WST assay was performed to evaluate the toxicity of dye **C3** to human glioma (A172) cells. The cells were seeded into 96-well plates at a cell density of 5×10^3 cells per well in 180 μL of culture medium and maintained for 24 h. Then a solution of dye **C3** with different concentrations

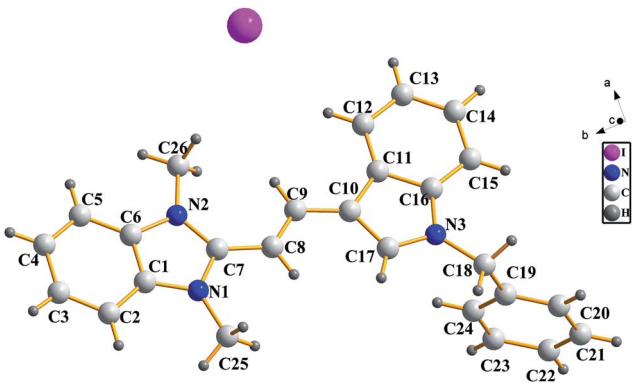

Fig. 1 The molecular structure diagram of dye **C2**.

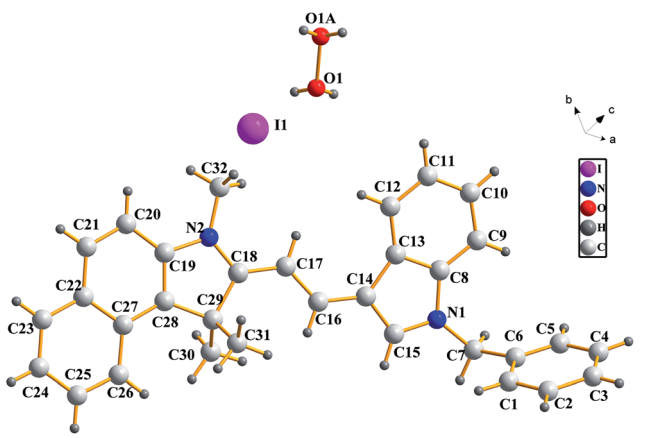

Fig. 2 The molecular structure diagram of dye **C6**.

Table 2 Crystal data and structure refinement for dyes C2 and C6

Dyes	C2	C6
Empirical formula	$C_{26}H_{24}IN_3$	$C_{33}H_{31}IN_2O$
Formula weight	505.38	598.50
Temperature (K)	298(2)	296(2)
Wavelength (Å)	0.71073	0.71073
Crystal system	Monoclinic	Monoclinic
Space group	*Pc*	*P*2(1)/*n*
Unit cell dimensions		
a (Å)	9.676(2)	12.3860(14)
b (Å)	5.8938(13)	10.3493(13)
c (Å)	19.693(4)	22.395(3)
α (deg)	90	90
β (deg)	94.577(3)	100.695(2)
γ (deg)	90	90
Volume (Å^3)	1119.5(4)	2820.9(6)
Z	2	4
Calculated density (mg m^{-3})	1.499	1.409
Absorption coefficient (mm^{-1})	1.448	1.163
F(000)	508	1216
Crystal size (mm^3)	0.35 × 0.27 × 0.17	0.32 × 0.26 × 0.13
θ range for data collection	2.07–25.10	1.85–25.10
Limiting indices *h*, *k*, *l*	−11/11, −3/7, −22/23	−14/14, −12/8, −26/24
Refinement method	Full-matrix least-squares on F^2	
Reflections collected/unique/R_{int}	5256/3649/0.0298	13 504/4921/0.0343
Completeness to θ =25.10°	99.8%	97.9%
Data/restraints/parameters	3649/2/273	4921/6/328
Goodness-of-fit on F^2	1.120	1.043
Final *R* indices [$I > 2\sigma(I)$]		
R_1	0.0417	0.0521
wR_2	0.1194	0.1346
***R* indices (all data)**		
R_1	0.0455	0.0785
wR_2	0.1336	0.1477
Largest difference peak/hole (e Å^{-3})	0.666 and −0.842	1.066 and −0.827

was added to 96-well plates and incubated for another 12 h. Following this, the medium was removed and washed three times with phosphate buffered saline (PBS). Finally, 100 μL of fresh culture medium and 10 μL of WST-1 reagent were added to each well. After incubation for 1 h, cell viability was measured using the WST assay according to the manufacturer's suggested procedure. All the experiments were conducted in triplicate. Data are expressed as mean ± standard deviation.

2.6.2 Fluorescence imaging. A172 cells were seeded into 24-well plates at a density of 1×10^4 cells per well and incubated for 12 h, and then dye **C3** was added. After further incubation for 10 min, the culture medium was washed three times with PBS. The fluorescence images were acquired using confocal laser scanning microscopy with an argon laser at an excitation wavelength of 488 nm and an emission wavelength of 570–620 nm.

3. Results and discussion

3.1 Synthesis

Six double *N*-alkylated dimethine cyanine dyes were synthesized *via* the nucleophilic addition–elimination reaction of *N*-benzyl-3-indole formaldehyde and quaternary ammonium salts having an active methyl group, with high yields of 59–84%, in short reaction times, and using an environmentally friendly method. The products were easily purified by recrystallization from EtOH or MeOH. In the synthetic process, it was found that the sequence of the reaction activity of various heterocyclic quaternary salts was benzimidazole quaternary salt < benzindole quaternary salt < benzothiazole quaternary salt < quinoline quaternary salt. This was because the reactivity of hydrogen in the active methyl groups differed from each other. The higher the reactivity of hydrogen, the easier it was to form a carbanion from the active methyl under basic conditions, and the easier the nucleophilic addition–elimination reaction of the quaternary salts and *N*-benzyl-3-indole formaldehyde was. However, the reactivity of hydrogen in an active methyl group was affected by the positive charge density of 2- or 4-carbon in a heterocyclic quaternary salts: the larger the positive charge density of the 2- or 4-carbon, the higher the reactivity of hydrogen. The electron-withdrawing ability of the group linked with a 2- or 4-carbon was –N(CH$_3$)– < –C(CH$_3$)$_2$– < –S– < –CH=CH–; therefore the positive charge density of the 2- or 4-carbon was benzimidazole

Table 3 Selected bond lengths (Å), bond angles and torsion angles (°) for dye C2

Bond lengths (Å)			
N(1)–C(7)	1.355(9)	N(3)–C(18)	1.473(9)
N(1)–C(1)	1.384(8)	C(7)–C(8)	1.455(8)
N(1)–C(25)	1.460(10)	C(8)–C(9)	1.333(9)
N(2)–C(7)	1.351(9)	C(9)–C(10)	1.419(9)
N(2)–C(6)	1.407(8)	C(10)–C(17)	1.400(10)
N(2)–C(26)	1.462(9)	C(10)–C(11)	1.461(9)
N(3)–C(17)	1.345(8)	C(11)–C(16)	1.431(10)
N(3)–C(16)	1.371(9)	C(18)–C(19)	1.522(11)
Bond angles (°)			
C(7)–N(1)–C(1)	108.7(5)	N(2)–C(7)–N(1)	108.1(5)
C(7)–N(1)–C(25)	127.9(6)	N(2)–C(7)–C(8)	130.0(6)
C(1)–N(1)–C(25)	123.3(6)	N(1)–C(7)–C(8)	121.8(6)
C(7)–N(2)–C(6)	108.9(5)	C(9)–C(8)–C(7)	127.9(6)
C(7)–N(2)–C(26)	127.9(5)	C(8)–C(9)–C(10)	123.7(6)
C(6)–N(2)–C(26)	123.2(5)	C(17)–C(10)–C(9)	127.5(6)
C(17)–N(3)–C(16)	110.1(5)	C(17)–C(10)–C(11)	106.1(6)
C(17)–N(3)–C(18)	124.1(6)	C(9)–C(10)–C(11)	126.4(7)
C(16)–N(3)–C(18)	125.8(6)	C(16)–C(11)–C(10)	105.2(6)
C(6)–C(1)–N(1)	108.1(5)	N(3)–C(16)–C(11)	108.4(5)
C(1)–C(6)–N(2)	106.2(5)	N(3)–C(17)–C(10)	110.1(6)
C(5)–C(6)–N(2)	131.7(6)	N(3)–C(18)–C(19)	114.2(7)
Torsion angles (°)			
N(1)–C(1)–C(6)–N(2)	0.0(6)	C(10)–C(11)–C(16)–N(3)	0.0(6)
C(6)–N(2)–C(7)–C(8)	179.5(6)	C(9)–C(10)–C(17)–N(3)	−178.1(6)
C(7)–C(8)–C(9)–C(10)	178.8(6)		

quaternary salt < benzindole quaternary salt < benzothiazole quaternary salt < quinoline quaternary salt, and the sequence of the reaction activity of the various heterocyclic quaternary salts was benzimidazole quaternary salt < benzindole quaternary salt < benzothiazole quaternary salt < quinoline quaternary salt.

Table 5 The geometry of D–H···A hydrogen bond of dye C2

D–H···A	d(D–H) (Å)	d(H···A) (Å)	d(D···A) (Å)	∠(DHA) (°)
C(17)–H(17)···I(1)	0.93	2.88	3.798(7)	168

3.2 Characterization

The purity of the prepared dyes **C1–C6** was established using HPLC and HPLC data obtained at particular wavelengths are presented in the ESI Fig. S1.† For each compound, the detection wavelength was set to 254 nm, 370 nm and its λ_{max}. As can be seen from the ESI,† the purity of the prepared dyes **C1–C6** is mostly above 99%. The structures of the six dyes were confirmed from UV-vis absorption spectra, IR, ^{1}H-NMR and HRMS. The IR spectra of the six dyes showed typical aromatic absorption ($\nu_{=C-H}$, 3091–3002 cm^{-1}, $\nu_{C=C}$, 1598–1536, $\delta_{=C-H}$, 964–719 cm^{-1}) and resonance conjugated unsaturated stretching modes ($\nu_{C=N}$, $\nu_{C=C}$, 1515–1448 cm^{-1}). Each dye also had a moderate absorption peak in the range of 964–939 cm^{-1}, which belonged to the *trans*-RCH=CRH chain. It indicated that these dyes had a *trans*-spatial configuration.[36] As can be seen from the ^{1}H-NMR spectra data, the coupling constants ($^3J_{HH}$) of hydrogen of the CH=CH chain were between 15.6–16.8 Hz, which further confirmed that these dye molecules had a *trans*-configuration. ^{1}H-NMR spectra of dyes **C1–C6** showed the chemical shift of H in N^+CH_3 (5.57–5.66 ppm), NCH_2 (4.15–4.49 ppm), CH=CH (7.16–8.04 ppm) and an aromatic heterocycle (7.30–9.15 ppm). The resonance absorption corresponding to $C(CH_3)_2$ (2.05 ppm)

Table 4 Selected bond lengths (Å), bond angles and torsion angles (°) for dye C6

Bond lengths (Å)			
N(1)–C(15)	1.332(5)	C(14)–C(16)	1.405(5)
N(1)–C(8)	1.398(5)	C(16)–C(17)	1.367(6)
N(1)–C(7)	1.472(5)	C(17)–C(18)	1.408(5)
N(2)–C(18)	1.315(5)	C(18)–C(29)	1.534(5)
N(2)–C(19)	1.411(5)	C(19)–C(28)	1.363(5)
N(2)–C(32)	1.465(5)	C(28)–C(29)	1.513(5)
C(8)–C(13)	1.407(5)	C(29)–C(30)	1.537(6)
C(13)–C(14)	1.456(5)	C(29)–C(31)	1.541(6)
C(14)–C(15)	1.384(6)		
Bond angles (°)			
C(15)–N(1)–C(8)	108.8(3)	C(17)–C(16)–C(14)	127.3(4)
C(18)–N(2)–C(19)	111.7(3)	C(16)–C(17)–C(18)	126.3(4)
N(1)–C(8)–C(13)	107.7(3)	N(2)–C(18)–C(17)	122.7(4)
C(8)–C(13)–C(14)	106.5(3)	N(2)–C(18)–C(29)	109.3(3)
C(15)–C(14)–C(16)	122.9(4)	C(17)–C(18)–C(29)	128.0(4)
C(15)–C(14)–C(13)	105.3(3)	C(28)–C(19)–N(2)	109.1(3)
C(16)–C(14)–C(13)	131.7(4)	C(19)–C(28)–C(29)	109.2(3)
N(1)–C(15)–C(14)	111.6(3)	C(28)–C(29)–C(18)	100.6(3)
Torsion angles (°)			
C(15)–N(1)–C(8)–C(13)	−1.0(4)	C(16)–C(17)–C(18)–N(2)	−179.7(4)
C(16)–C(14)–C(15)–N(1)	176.1(4)	C(18)–N(2)–C(19)–C(28)	−2.5(4)
C(14)–C(16)–C(17)–C(18)	−179.4(4)		

Table 6 The absorption and fluorescence spectral characteristics of dyes **C1–C6** in different solvents

Solvents	Dyes	λ_{max} (nm)	λ_{ex} (nm)	λ_{em} (nm)	Stokes shift (nm)	$\varepsilon \times 10^{-4}$ (L mol^{-1} cm^{-1})	Φ^a
H_2O	**C1**	455.0	455.0	525.0	70.0	1.98	0.0676
	C2	368.0	368.0	468.2	100.2	0.89	0.0042
	C3	473.0	473.0	574.0	101.0	1.91	0.0332
	C4	468.0	468.0	561.6	93.6	2.80	0.0157
	C5	458.0	458.0	554.2	96.2	3.52	0.0264
	C6	483.0	483.0	560.0	77.0	3.24	0.0843
DMSO	**C1**	471.0	471.0	534.8	63.8	3.17	0.5705
	C2	378.0	378.0	469.8	91.8	0.87	0.0115
	C3	503.0	503.0	596.6	93.6	2.09	0.4572
	C4	492.0	492.0	570.4	78.4	2.98	0.1206
	C5	481.0	481.0	565.0	84.0	3.21	0.2103
	C6	491.0	491.0	560.8	69.8	3.26	0.2758
MeOH	**C1**	471.0	471.0	536.8	65.8	3.30	0.1643
	C2	376.0	376.0	471.2	95.2	0.97	0.0043
	C3	503.0	503.0	581.6	78.6	2.28	0.1507
	C4	491.0	491.0	564.2	73.2	3.25	0.0501
	C5	479.0	479.0	558.4	79.4	4.13	0.1261
	C6	489.0	489.0	558.4	69.4	3.53	0.0765
EtOH	**C1**	475.0	475.0	534.4	59.4	3.35	0.2309
	C2	380.0	380.0	460.6	80.6	0.98	0.0040
	C3	509.0	509.0	582.4	73.4	2.33	0.3614
	C4	494.0	494.0	563.2	69.2	3.66	0.1496
	C5	483.0	483.0	561.4	78.4	3.31	0.2644
	C6	493.0	493.0	563.2	71.2	3.44	0.1120
$CHCl_3$	**C1**	496.0	496.0	555.8	59.8	3.27	0.1672
	C2	384.0	384.0	471.4	87.4	0.78	0.0024
	C3	513.0	513.0	570.0	57.0	2.82	0.2573
	C4	515.0	515.0	577.2	62.2	3.29	0.1367
	C5	503.0	503.0	568.0	65.0	2.16	0.1669
	C6	522.0	522.0	573.4	51.4	2.34	0.0368

[a] The fluorescence quantum yields of the dyes were determined using the reference standard (rhodamine B $\Phi_F = 0.56$ in EtOH at 25 °C).[40]

was also found in dye **C6**. The HRMS data of dyes **C1–C6** showed that the relative molecular mass of the six dyes was consistent with the theoretical calculation results, and the error was less than 5 ppm.

3.3 Crystal structure

3.3.1 Description of crystal structure. The molecular structures and atom numbering of dyes **C2** and **C6** are shown in Fig. 1 and 2, and their bond lengths, bond angles and torsion angles are listed in Tables 3 and 4. From the tables, it was found that the carbon–carbon bond lengths of the molecular framework of dyes **C2** and **C6** were basically intermediate between typical C–C single (1.54 Å) and C=C double (1.34 Å) bonds and the carbon–nitrogen bond lengths were also basically intermediate between typical C–N single (1.47 Å) and C=N double (1.27 Å) bonds. It meant that the bond lengths of the carbon–carbon and carbon–nitrogen on the dye molecular skeleton had a tendency of averaging, and the π electrons in the dye molecular framework were delocalized. All bond angles were close to 108° in five-membered rings and close to 120° in benzene rings, which illustrated that the heterocycle skeleton of both **C2** and **C6** had no deformation. For dye **C2**, the torsion angles of C(8)–C(9)–C(10)–C(11), C(8)–C(9)–C(10)–C(17), N(2)–C(7)–C(8)–C(9) and N(1)–C(7)–C(8)–C(9) were −178.8°, −1.0°, −0.8° and 177.0°, respectively, which showed that the indole ring, vinyl chains and benzimidazole ring were basically in the same plane. It could also be seen that the two methyl groups and the imidazole ring were in the same plane, while the benzene ring in benzyl group was distorted from coplanarity with the indole ring. For dye **C6**, the torsion angles of C(13)–C(14)–C(16)–C(17), C(15)–C(14)–C(16)–C(17), C(16)–C(17)–C(18)–N(2) and C(16)–C(17)–C(18)–C(29) were 6.8°, −170.6°, −179.7° and 3.6°, respectively, which showed that the indole ring and benzindole ring were slightly reversed, and not entirely in the same plane.

3.3.2 Crystal packing. The crystal packing of dye **C2** along the *a* axis and **C6** along the *b* axis are shown in Fig. 3 and 4. Dyes **C2** and **C6** crystallized in the monoclinic *Pc* space groups with two dye molecules per unit cell and monoclinic $P2_1/n$ space groups with four dye molecules and one water molecule per unit cell, respectively. For dye **C2**, in the crystal packing along the *a* axis, there was one type of hydrogen bond between the molecules, that is C(17)–H(17)·I(1), formed by C(17)–H(17) in the indole ring from one molecule and I(1) from another molecule (Table 5), which made dye molecules form a layered structure in the *bc* plane. As can be seen from the packing diagrams of **C2** (Fig. 3), adjacent molecules were stacked through the π–π interaction force, with face-to-face distances of 3.492 Å and the conjugated molecules were arranged in a

Table 7 The fluorescence quantum yields of dyes **C1–C6** with different biomolecules[a]

Dyes	Dye concentrations (mol L^{-1})	Biomolecules concentrations (μg mL^{-1})	DNA Φ/Φ_{free}	BSA Φ/Φ_{free}	Muramidase Φ/Φ_{free}	Amylase Φ/Φ_{free}	Chymotrypsin Φ/Φ_{free}	Bovine hemoglobin Φ/Φ_{free}
C1	1×10^{-5}	0	1.00	1.00	1.00	1.00	1.00	1.00
		4	6.83	0.97	1.13	0.98	1.23	0.97
		10	15.36	0.87	0.93	0.74	0.93	0.90
	5×10^{-5}	0	1.00	1.00	1.00	1.00	1.00	1.00
		4	0.84	0.85	1.00	0.96	0.92	0.87
		10	1.45	0.85	0.98	0.92	0.94	0.84
C2	1×10^{-5}	0	1.00	1.00	1.00	1.00	1.00	1.00
		4	0.63	0.80	0.33	0.39	0.33	0.35
		10	0.71	0.72	0.28	0.36	0.31	0.16
	5×10^{-5}	0	1.00	1.00	1.00	1.00	1.00	1.00
		4	0.69	0.98	0.47	0.28	0.27	0.39
		10	0.66	0.93	0.36	0.34	0.27	0.33
C3	1×10^{-5}	0	1.00	1.00	1.00	1.00	1.00	1.00
		4	0.79	0.92	0.96	0.94	0.94	0.88
		10	3.75	0.80	0.88	0.73	0.88	0.78
	3×10^{-5}	0	1.00	1.00	1.00	1.00	1.00	1.00
		4	1.11	0.97	0.98	1.06	0.94	0.81
		10	0.40	0.79	0.77	1.00	0.90	0.96
C4	1×10^{-5}	0	1.00	1.00	1.00	1.00	1.00	1.00
		4	1.16	0.74	0.87	0.80	0.86	0.80
		10	5.43	0.77	0.77	0.59	0.76	0.75
	3×10^{-5}	0	1.00	1.00	1.00	1.00	1.00	1.00
		4	0.34	0.53	0.74	0.90	0.64	0.46
		10	0.28	0.48	0.63	0.75	0.47	0.47
C5	1×10^{-5}	0	1.00	1.00	1.00	1.00	1.00	1.00
		4	3.76	0.91	1.11	1.16	0.98	0.98
		10	8.94	1.08	0.92	1.62	0.94	1.04
	3×10^{-5}	0	1.00	1.00	1.00	1.00	1.00	1.00
		4	2.97	0.84	1.17	2.96	0.75	2.28
		10	3.65	0.91	1.70	1.16	0.83	0.77
C6	5×10^{-6}	0	1.00	1.00	1.00	1.00	1.00	1.00
		4	0.99	0.81	0.90	0.93	0.85	0.59
		10	1.35	0.92	0.83	1.18	0.80	0.79
	1×10^{-5}	0	1.00	1.00	1.00	1.00	1.00	1.00
		4	1.20	0.96	0.98	1.05	1.06	0.97
		10	1.44	0.99	0.98	1.14	0.91	0.96

[a] Φ: the fluorescence quantum yields of dye in the presence of biomolecule; Φ_{free} the fluorescence quantum yields of pure dye.

head-to-head fashion along the *a* axis. The coulombic attraction between I^- in one molecule and N^+ in adjacent molecules stabilized the molecular packing, whose distance of I^- and N^+ of adjacent dye molecules was 5.133 Å and 4.885 Å, respectively. In this manner, molecular interactions, including hydrogen bonds, π–π interaction force and coulombic attraction, made the dye molecules form a steric configuration of a three-dimensional framework. For dye **C6**, in the same layer of the packing crystal structure, the dye molecules were stacked face-to-face along the *b* axis through coulombic attraction between I^- and N^+, with the distance of 3.909 Å and 4.940 Å, respectively. In summary, the existence of coulombic attraction stabilized the steric configuration.

3.4 Spectral properties

3.4.1 Spectral properties of dyes C1–C6 in different solvents. The absorption spectral data of six dyes in different solvents are listed in Table 6. It was found that the maximum absorption wavelengths (λ_{max}) and the molar extinction coefficient of dyes **C1–C6** were located in the range of 368.0–522.0 nm and 0.78×10^4 to 4.13×10^4 L mol^{-1} cm^{-1}, respectively. The sequence of the λ_{max} of six dyes was **C6** > **C3**, **C4**, **C5** > **C1** > **C2** in the same solvent. The reason for this was that the λ_{max} was related to the size of the conjugated system of dyes: the greater the conjugated system, the greater the λ_{max}. In the donor–π–acceptor (D–π–A) conjugated structure of dyes **C1–C6**, their electron donor was the same, whereas the electron acceptor was different and their size of conjugated fragments was benzoindoleninium > quinolinium > benzothiazolium > benzimidazolium. Therefore, the size of the conjugated system for dyes **C1–C6** was in the order **C6** > **C3**, **C4**, **C5** > **C1** > **C2**, leading to a ranking for λ_{max} of **C6** > **C3**, **C4**, **C5** > **C1** > **C2** in the same solvent. The experimental results also found that the λ_{max} of dyes **C1–C6** was increased with a decrease in the basicity of the heterocyclic nucleus (the sequence of the basicity of heterocyclic nucleus was benzindole < quinoline < benzothiazole < benzimidazole), which was consistent with results in the literature.[37]

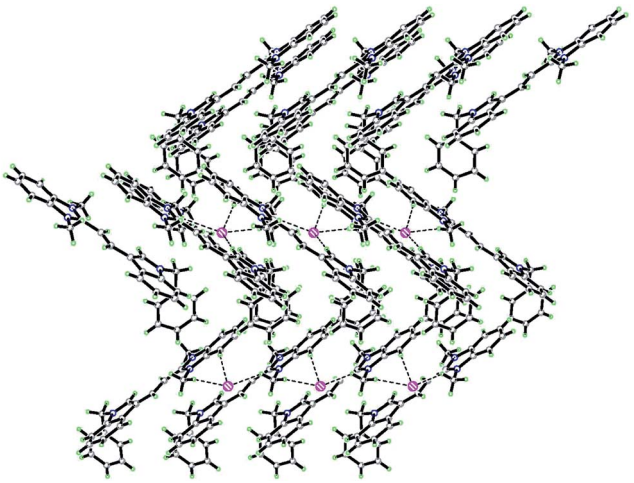

Fig. 3 Crystal packing of dye **C2** along the *a* axis.

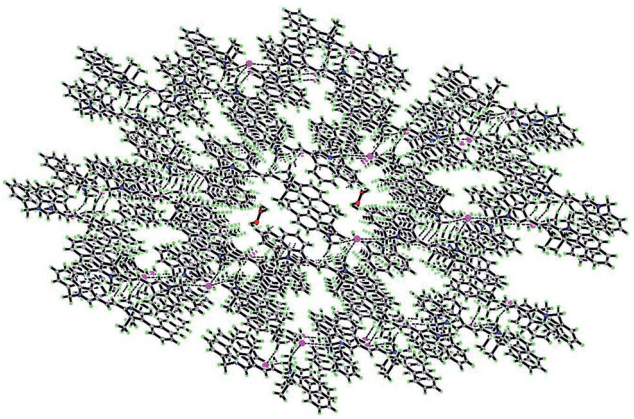

Fig. 4 Crystal packing of dye **C6** along the *b* axis.

Fig. 5 shows the λ_{max} of dyes **C1–C6** in different solvents (their dielectric constant: chloroform ($CHCl_3$) 4.8, EtOH 24.6, MeOH 32.6, DMSO 48.9, H_2O 78.4). It could be seen that the sequence of the λ_{max} of the same dye in protonic solvent and non-protonic solvent was λ_{max}(EtOH) > λ_{max}(MeOH) > λ_{max}(H_2O) and λ_{max}($CHCl_3$) > λ_{max}(DMSO). That is, with the increase of the dielectric constant of solvents, the λ_{max} of dyes was hypsochromic-shifted. The reason for this was that there was strong interaction between the solvent molecules with a large dielectric constant and the dye molecules, making the ground state energy of the dye molecules lower and the transition energy of dye molecules increase, consequently resulting in a blue shift in the λ_{max} of dyes.[38]

At the same time, from the absorption spectra of dyes **C1–C6** in different solvents (see ESI†), it was also found that six dyes mainly existed in the monomer form (M) in H_2O, MeOH, EtOH and DMSO, and dyes **C1** and **C4–C6** happened to aggregate in $CHCl_3$, especially **C1** which was mainly in H-aggregated states, which were attributed to the structure of the dye and the viscosity of the solvent.[39] And from the preparation of the dye solutions it was found that six dyes had good solubility in

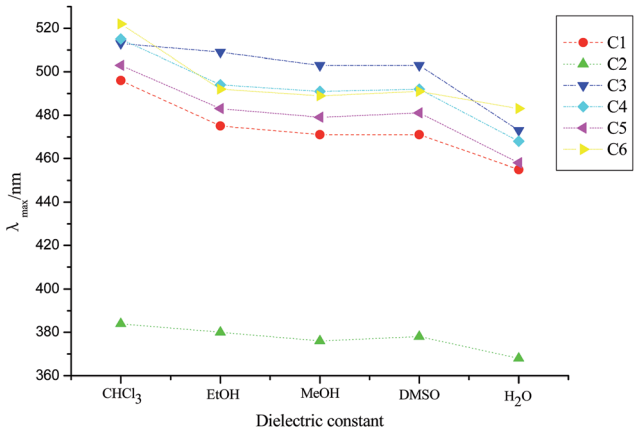

Fig. 5 The λ_{max} of dyes **C1–C6** in different solvents.

DMSO, and had considerable solubility in H_2O, MeOH, EtOH and $CHCl_3$.

The fluorescence spectral characteristics of dyes **C1–C6** in different solvents are shown in Table 6. As indicated in the table, all six dyes fluoresced in H_2O, MeOH, EtOH, $CHCl_3$ and DMSO. The fluorescence maximum emission wavelength (λ_{em}) ranged from 460.6 to 596.6 nm in different solvents, and a bathochromic shift had occurred at 51.4–101.0 nm (Stokes shift), when compared with the corresponding absorption maxima; furthermore, the Stokes shift of the six dyes was largest in H_2O, followed by DMSO, which was beneficial for the biological study. The sequence of the fluorescence quantum yields[40] in three protonic solvents was Φ(EtOH) > Φ(MeOH) > Φ(H_2O). This was because the electron cloud in the conjugated system was dispersed as the solvent polarity increased, which resulted in a strong intramolecular charge transfer, leading to fluorescence quenching.[41]

3.4.2 The interaction of dyes C1–C6 with biomolecules. The interaction between the dye molecules and six biological molecules including DNA, BSA, muramidase, amylase, bovine hemoglobin and chymotrypsin, was investigated to explore the possibility of their use as biological fluorescent probes. The detailed spectral properties of dyes **C1–C6** with different biomolecules are shown in Table 7. It was found that the fluorescence quantum yields of six dyes had amplitude changes when six kinds of biological molecules were added, but the fluorescence quantum yield of dye **C1** at 1×10^{-5} mol L^{-1} showed a significant increase when adding 10 μg mL^{-1} DNA. Therefore, the interaction between dye **C1** and DNA is now discussed in detail.

The UV-vis absorption and fluorescence spectral data of dye **C1** with DNA and the changes of fluorescence intensity with the concentration of DNA are presented in Table 8 and Fig. 6, respectively. It can be seen that the molar extinction coefficient of dye **C1** was decreased in the presence of DNA (Table 8), and it also showed a hypochromic effect, which indicated that the dye **C1** was inserted into the DNA molecule.[42] As can be seen from Fig. 6 and Table 8, the λ_{em} of the dye displayed a red-shift in the presence of DNA, and the

Table 8 The spectroscopic data of dye **C1** in the presence of DNA

		Absorption			Fluorescence			
Dye	DNA concentration (μg mL^{-1})	λ_{max} (nm)	Hypochromic effect (%)	$\varepsilon \times 10^{-4}$ (L mol^{-1} cm^{-1})	λ_{ex} (nm)	λ_{em} (nm)	Stokes shifts (nm)	Φ_{DNA}/Φ_{free}
C1	0	445.0	0.0	3.18	455.0	521.6	66.6	1.00
	2	454.0	11.3	2.82	455.0	526.6	71.6	4.00
	4	460.0	33.6	2.11	455.0	525.0	70.0	6.83
	6	466.0	23.9	2.42	455.0	525.8	70.8	9.46
	8	468.0	23.3	2.44	455.0	525.2	70.2	12.77
	10	463.0	29.6	2.24	455.0	525.4	70.4	15.36
	12	466.0	19.8	2.55	455.0	525.4	70.4	15.57

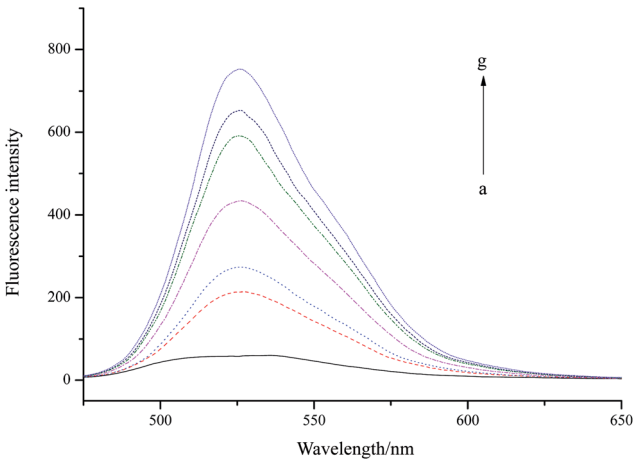

Fig. 6 Fluorescence spectra of dye **C1** (1×10^{-5} mol L^{-1}) with different concentrations of DNA.

fluorescence intensity and fluorescence quantum yield of the dye were increased linearly with increasing concentration of DNA. This was because when the aromatic ring plane of the dye was inserted into the base pairs of DNA, the dye molecules were protected by the DNA hydrophobic effect, which made the fluorescence quenching of dye caused by the solvent molecules become weak and the fluorescence intensity was increased.[43] Because of the packing of π electrons between base pairs and dye molecules, and the coupling effect of the empty π* orbital of dye and the π orbital of base pairs, the energy level of the π* orbital of the dye molecules was lowered, and the transition energy of π* → π was reduced, leading to the red-shift of the λ_{em} of dye.[44,45]

3.5 Cytotoxicity and cell staining of dye C3

For biomedical applications such as fluorescent probes and cellular imaging, the toxicity of the dye was a major concern. To assess the cytotoxicity of the selected dye **C3**, a WST assay was performed with A172 cell lines. The results (Fig. 7) indicated that the cell viability of dye **C3** was more than 87% at the application dose and duration, suggesting a very low cytotoxicity of dye **C3**.

The cell staining of dye **C3** was also investigated by fluorescence imaging. A172 cells were incubated with dye **C3** at a concentration of 20 μmol L^{-1} for 10 min and the reaction was observed using fluorescence microscopy. As shown in Fig. 8, strong fluorescence (excitation at 488 nm, emission wavelength of 570–620 nm) was observed in A172 cells, suggesting that dye **C3** could stain A127 cells, and that the dye was mainly distributed in the cytoplasm. The results indicated that dye **C3** would be able to act as a potential fluorescent reagent to clearly observe cells, for the determination of the characteristics of cells and the developmental stages of cells. Further

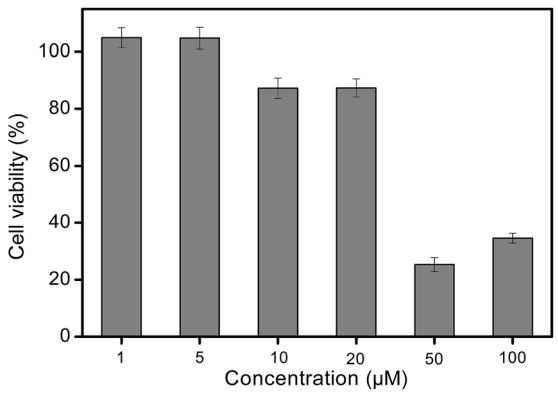

Fig. 7 The viability of A172 cells incubated with dye **C3** at various concentrations for 12 h. Error bars are based on triplicate samples.

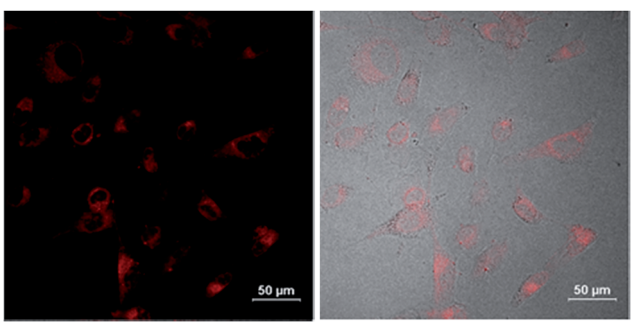

Fig. 8 Confocal fluorescence microscopic images of A172 cells incubated with dye **C3** at 37 °C for 10 min. Scale bar: 50 μm.

investigation of cytotoxicity and cell staining of the other dyes synthesized is in progress.

4. Conclusions

Six new double *N*-alkylated dimethine cyanine dyes were synthesized using, as starting materials, *N*-benzyl-3-indole formaldehyde and heterocyclic quaternary ammonium salts having an active methyl group. The products were confirmed using UV-vis, IR, HRMS, ^{1}H-NMR. The single XRD of **C2** and **C6** revealed that the two dyes crystallized in the monoclinic *Pc* with $a = 9.676$ Å, $b = 5.8938$ Å, $c = 19.693$ Å, $V = 1119.5$ Å^3, $Z = 2$ and monoclinic $P2_1/n$ with $a = 12.3860$ Å, $b = 10.3493$ Å, $c = 22.395$ Å, $V = 2820.9$ Å^3, $Z = 4$ space groups, respectively, and the crystal packing was stabilized by hydrogen bonds, π–π stacking interactions and coulombic attractions. The absorption maxima and the molar extinction coefficient of the dyes were located in the range of 368.0–522.0 nm and 0.78×10^4 to 4.13×10^4 L mol^{-1} cm^{-1} in different solvents, respectively. The fluorescence maxima and Stokes shift of the dyes ranged from 460.6 to 596.6 nm and from 51.4 to 101.0 nm in different solvents, respectively, and dyes **C1** and **C3** showed a relatively high fluorescence quantum yield. The interaction between these dye molecules and six biological molecules showed that there was larger enhancement of fluorescent quantum yield for dye **C1** in the presence of DNA. The investigation of the cytotoxicity and cell staining of the selected dye **C3** revealed virtually no toxicity at the dose and duration applied and demonstrated that the dye could stain cytoplasm. It is suggested that this dye is a potential fluorescent reagent for observing cells clearly, and for determining their characteristics and developmental stages.

Acknowledgements

We appreciate the financial support for this research from a grant from the Scientific and Technological Research and Development Projects in Shaanxi Province (2012K07-06) and the Special Science Research Foundation of Education Committee (no. 11JK0558).

References

1 B. Fan, F. A. de Castro, J. Heier, R. Hany and F. Nüesch, *Org. Electron.*, 2010, **11**, 583–588.
2 G. Wicht, S. Bücheler, M. Dietrich, T. Jägerb, F. Nüesch, T. Offermans, J. N. Tisserant, L. Wang, H. Zhang and R. Hany, *Sol. Energy Mater. Sol. Cells*, 2013, **117**, 585–591.
3 H. Zhang, G. Wicht, C. Gretener, M. Nagel, F. Nüesch, Y. Romanyuk, J. N. Tisserant and R. Hany, *Sol. Energy Mater. Sol. Cells*, 2013, **118**, 157–164.
4 Y. Yang, S. Omi, R. Goto, M. Yahiro, M. Era, H. Watanabe and Y. Oki, *Org. Electron.*, 2011, **12**, 405–410.
5 D. D. Nolting, J. C. Gore and W. Pham, *Curr. Org. Synth.*, 2011, **8**, 521–534.
6 A. Winstead and R. Williams, *Environ. Biosens.*, 2011, **11**, 237–254.
7 S. Dash, M. Panigrahi, S. Baliyarsingh, P. K. Behera, S. Patel and B. K. Mishral, *Curr. Org. Chem.*, 2011, **15**, 2673–2689.
8 S. M. Yarmoluk, V. B. Kovalska and K. D. Volkova, Optimized Dyes for Protein and Nucleic Acid Detection, *Springer Ser. Fluoresc.*, 2011, **10**, 161–200.
9 J. Kabatc, A. Bajorek and R. Dobosz, *J. Mol. Struct.*, 2011, **985**, 95–104.
10 L. Glavaš-Obrovac, I. Piantanida, S. Marczi, L. Mašić, I. I. Timcheva and T. G. Deligeorgiev, *Bioorg. Med. Chem.*, 2009, **17**, 4747–4755.
11 P. Hanczyc, B. Norden and B. Âkerman, *J. Phys. Chem. B*, 2011, **115**, 12192–12201.
12 S. Kaloyanova, I. Crnolatac, N. Lesev, I. Piantanida and T. G. Deligeorgiev, *Dyes Pigm.*, 2012, **92**, 1184–1191.
13 T. G. Deligeorgiev, A. Vasilev and K. Drexhage, *Dyes Pigm.*, 2007, **74**, 320–328.
14 N. I. Shank, H. H. Pham, A. S. Waggoner and B. A. Armitage, *J. Am. Chem. Soc.*, 2013, **135**, 242–251.
15 Y. Kimura, T. Hanami, M. J. de Hoon, T. Soma, M. Harbers, A. Lezhava, Y. Hayashizaki and K. Usui, *Biochemistry*, 2012, **51**, 6056–6067.
16 K. Lee, K. Maisel, J. Rouillard, E. Gulari and J. Kim, *Chem. Mater.*, 2008, **20**, 2848–2850.
17 E. J. Fechter, B. Olenyuk and P. B. Dervan, *J. Am. Chem. Soc.*, 2005, **127**, 16685–16691.
18 C. Holzhauser, R. Liebl, A. Goepferich, H. A. Waqenknecht and M. Breunig, *Chem. Biol.*, 2013, **8**, 890–894.
19 Y. Kam, A. Rubinstein, A. Nissan, D. Halle and E. Yavin, *Mol. Pharmaceutics*, 2012, **9**, 685–693.
20 T. G. Deligeorgiev, A. Vasilev and K. Drexhage, *Dyes Pigm.*, 2007, **73**, 69–75.
21 Y. L. Fu, B. R. Zhang, S. Wang, X. X. Gao and L. Y. Wang, *Bull. Korean Chem. Soc.*, 2013, **2**, 489–494.
22 L. Glavaš-Obrovac, I. Piantanida, S. Marczi, L. Masic, I. I. Timcheva and T. G. Deligeorgiev, *Bioorg. Med. Chem.*, 2009, **17**, 4747–4755.
23 X. H. Zhang, L. Y. Wang, Z. X. Nan, S. H. Tan and Z. X. Zhang, *Dyes Pigm.*, 2008, **79**, 205–209.
24 S. L. Wang and Y. T. Chang, *J. Am. Chem. Soc.*, 2006, **128**, 10380–10381.
25 Q. Li, Y. Kim, J. Namm, A. Kulkarni, G. R. Rosania and Y. T. Chang, *Chem. Biol.*, 2006, **13**, 615–623.
26 R. M. Abd El-Aal, A. I. M. Koraiem, Z. H. Khalil and A. M. M. El-Kodey, *Dyes Pigm.*, 2005, **66**, 201–209.
27 T. G. Deligeorgiev, N. Gadjev, S. Kaloyanova, N. Lesev, A. Vasilev and A. Alexiev, *Color. Technol.*, 2012, **128**, 417–424.
28 X. H. Zhang, L. Y. Wang, G. H. Zhai, Z. Y. Wen and Z. X. Zhang, *Bull. Korean Chem. Soc.*, 2007, **28**, 2382–2388.
29 X. H. Zhang, Q. Liu, H. J. Shi, Y. L. Fu, X. C. Wei, L. Y. Wang, Y. L. Fu, X. C. Wei and L. F. Yang, *Dyes Pigm.*, 2014, **100**, 232–240.
30 S. A. Hilderbrand and R. Weissleder, *Chem. Commun.*, 2007, **26**, 2747–2749.
31 N. J. Leonard, H. A. Dewalt Jr and G. W. Leubner, *J. Am. Chem. Soc.*, 1951, **73**, 3325–3329.
32 Q. Kang, F. L. Fan, W. B. Bi, Y. Huang, Y. L. Fu and L. Y. Wang, *Chin. J. Org. Chem.*, 2012, **32**, 567–573.

33 C. Sagnes, G. Fournet and B. Joseph, *Synlett*, 2009, **3**, 433–436.
34 G. M. Sheldrick, *SHELXS-97, Program for Solution Crystal Structure*, University of Göttingen, Germany, 1997.
35 G. M. Sheldrick, *SHELXL-97, Program for Solution Crystal Structure and Refinement*, University of Göttingen, Germany, 1997.
36 J. H. Chang and Q. G. Dong, *The principle and parsing of spectrum*, Science Press, Beijing, 1st edn, 2001, pp. 76–152.
37 L. G. S. Brooker By, A. L. Sklar, H. W. J. Cressman, G. H. Keyes, L. A. Smith, R. H. Sprague, E. Van Lare, G. Van Zandt, F. L. White and W. W. Willams, *J. Am. Chem. Soc.*, 1945, **67**, 1875–1889.
38 R. M. El-Shishtawy, A. M. Asiri, S. A. Basaif and T. Rashad Sobahi, *Spectrochim. Acta, Part A*, 2010, **75**, 1605–1609.
39 F. M. Hamer, *The cyanine dyes and related compound*, Interscience interscience publishers, New York, 1964, p. 716.
40 T. Karstens and K. Kobs, *J. Phys. Chem.*, 1980, **84**, 1871–1872.
41 C. Zhao, H. Y. Ge and P. Han, *Chem. Ind. Times*, 2010, **24**, 4–8.
42 B. Y. Wu, L. H. Gao and K. Z. Wang, *Chem. Res. Chin. Univ.*, 2005, **26**, 1206–1209.
43 J. Fan, L. F. Wang and Q. Kong, *J. Shaanxi Norm. Univ., Nat. Sci. Ed.*, 2007, **35**, 76–79.
44 R. Indumathy, S. Radhika, M. T. Kanthimathi, T. Weyhermuller and B. U. Nair, *J. Inorg. Biochem.*, 2007, **101**, 434–443.
45 S. Satyanarayana, J. C. Dabrowiak and J. B. Chaires, *Biochemistry*, 1992, **31**, 9319–9324.